

Lawrence Berkeley National Laboratory

Lawrence Berkeley National Laboratory

Title

Measurement of the Intensity of the Cosmic Background Radiation at 3.7 GHz

Permalink

<https://escholarship.org/uc/item/24x9x9dt>

Authors

De Amici, G.
Smoot, G.F.
Aymon, J.
et al.

Publication Date

1987-04-01

LB Lawrence Berkeley Laboratory
UNIVERSITY OF CALIFORNIA

Physics Division

RECEIVED
LAWRENCE
BERKELEY LABORATORY

JUL 9 1987

LIBRARY AND
DOCUMENTS SECTION

Submitted to Astrophysical Journal

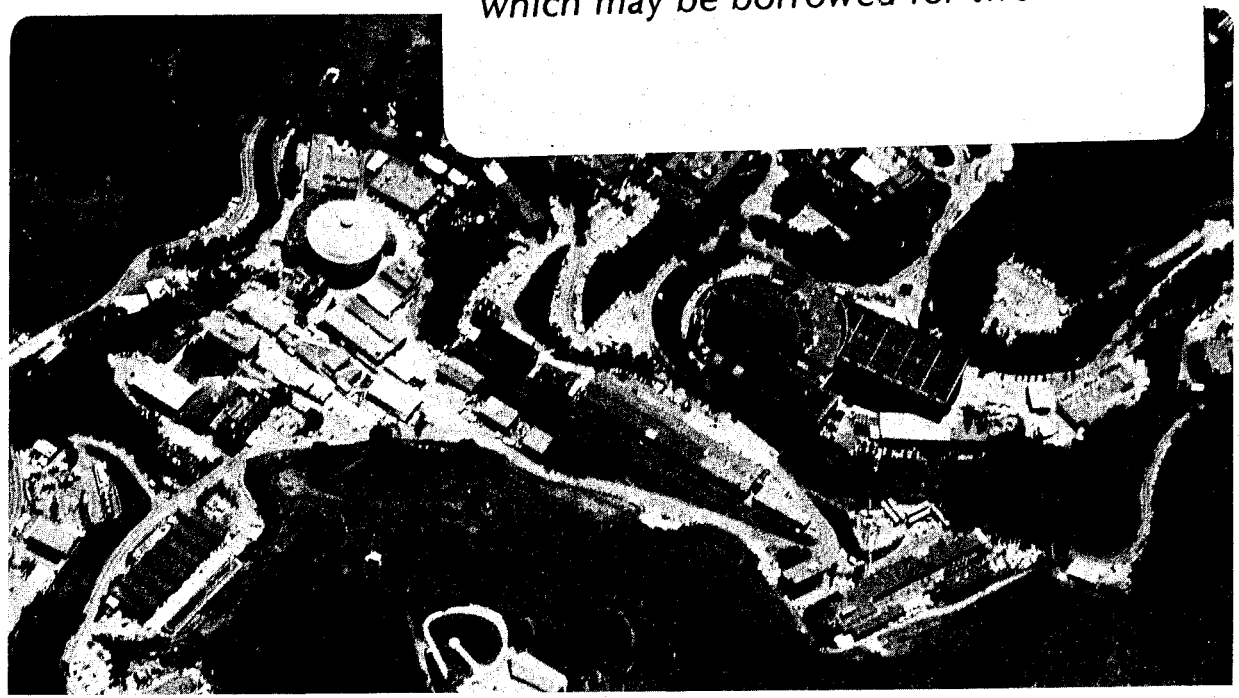
**MEASUREMENT OF THE INTENSITY OF THE
COSMIC BACKGROUND RADIATION AT 3.7 GHz**

G. De Amici, G.F. Smoot, J. Aymon,
M. Bersanelli, A. Kogut, S.M. Levin,
and C. Witebsky

April 1987

TWO-WEEK LOAN COPY

*This is a Library Circulating Copy
which may be borrowed for two weeks.*



LBL-23300
e2

**Measurement of the Intensity of the
Cosmic Background Radiation at 3.7 GHz**

Giovanni De Amici, George F. Smoot, Jon Aymon,
Marco Bersanelli, Al Kogut, Steven M. Levin, Chris Witebsky

Lawrence Berkeley Laboratory and Space Sciences Laboratory
University of California, Berkeley, CA 94720

ABSTRACT

We measured the temperature of the cosmic background radiation (CBR) at a frequency of 3.7 GHz (8.1 cm wavelength), using a total power, direct RF-gain receiver. The results give a brightness temperature, T_{CBR} , of 2.58 ± 0.13 K (68% C.L.). Details of the instrument and of the experimental procedure are given. This measurement is part of a larger experiment to measure the spectrum of the Cosmic Background Radiation between 0.6 and 90 GHz (50 and 0.33 cm wavelength).

subject headings: cosmic background radiation

I. INTRODUCTION

Shortly after its discovery (Penzias and Wilson 1965), the spectrum of the cosmic background radiation (CBR) was subject to extensive measurements to determine its shape. Within a couple of years, however, the interest in low-frequency spectral measurements largely disappeared, and did not resurface until recent times. The high-frequency spectrometer flown by Woody and Richards (1981), and the theoretical analysis of their data that followed (e.g. Danese and De Zotti 1982, and references therein) suggested the possibility that the spectral shape in the Rayleigh-Jeans region could contain information about the history of the universe in the epochs immediately before and during the formation of galaxies and clusters of galaxies.

An international collaboration composed of our group at Berkeley and researchers from Haverford (Pennsylvania), Bologna, Milano and Padova (Italy) has performed measurements of the low frequency spectrum of the CBR using ground based receivers (Smoot *et al.* 1985a). Since the end of the collaboration, the Berkeley and Milano groups have continued the effort. Our previous data, combined with those by Meyer and Jura (1984) and Peterson *et al.* (1985) at higher frequencies, rule out distortions to the 6% level (Smoot *et al.* 1985a) in the frequency range between a few GHz and the peak of the blackbody distribution. Therefore we added new low-frequency receivers to improve spectral coverage, and to reduce the limits on possible distortions in the CBR.

The 3.7 GHz frequency was chosen because of the availability of high performance commercial amplifiers. A suitable antenna was already available through the Bologna/CNR group, and the choice of a frequency close to a recently measured point (4.75 GHz) allows us to

compare this result with those obtained, from the same location, by Mandolesi *et al.* (1984, 1986).

II. CONCEPT OF MEASUREMENT

The radiometer is a microwave receiver whose output signal is proportional to the input power, P , per unit bandwidth, B . This quantity can be measured in units of antenna temperature, T_A . For a blackbody at a temperature T covering the antenna aperture, the antenna temperature is:

$$T_A = \frac{P}{kB} = \frac{T_V}{e^{T_V/T} - 1}$$

where $T_V = h\nu/k = 0.178$ K at 3.7 GHz, h is Plank's constant, ν is frequency, and k is Boltzmann's constant.

Each measurement consists of the comparison of the antenna temperatures of the zenith sky and of an absolute reference cold load. The cold load is a layer of Eccosorb (an almost perfect black-body absorber at microwave frequencies) covering the bottom of a large (70 cm wide, 150 cm deep) dewar, which is filled with a cryogenic liquid (LHe), so that the absorber is completely submerged. When the receiver is looking vertically at the sky, the signal received (T_{zenith}) is the sum of many contributions:

$$T_{zenith} = T_{A,CBR} + T_{A,galaxy} + T_{A,ground} + T_{A,atm} \quad (1)$$

where the attenuation due to the atmosphere ($\approx 0.3\%$) has been neglected in this discussion, but not in the analysis, and $T_{A,CBR}$, $T_{A,galaxy}$, $T_{A,ground}$, and $T_{A,atm}$ are respectively the antenna temperatures of the CBR, the galaxy, the ground seen through the antenna sidelobes, and the atmosphere. The difference in radiometer output when looking at the sky or at the cold load is

$$G (S_{zenith} - S_{load}) = T_{zenith} - T_{A,load} + \Delta T_{sys} + \frac{\Delta G}{G} T_{A,load} + \frac{\Delta G}{G} T_{sys} \quad (2)$$

where G is the receiver's calibration constant, S is the output signal when viewing the zenith or the cold load, $\Delta G/G$ is the fractional change in calibration constant when the receiver is moved from up to down, and ΔT_{sys} is any position-dependent change in receiver's system temperature ($\Delta T_{sys} = T_{sys}(\text{up}) - T_{sys}(\text{down})$). T_{sys} is the receiver output for a zero-temperature input. The last three terms in eq. (2) can be measured by rotating the radiometer up and down, and looking at its output with warm and cold loads. However, it is impractical to make a stable cold load that can be rotated up and down. A warm load alone does not allow us to differentiate between changes in system temperature or calibration constant. In each case where an ambiguity was possible, we took a worst case scenario. As will be shown later, the last two terms in eq. (2) are negligible for this radiometer.

III. DESCRIPTION OF INSTRUMENT

The instrument used for this experiment is a total power, direct RF-gain radiometer. It consists of an antenna, a front-end RF amplifier, a 3.5 GHz high-pass filter, a second stage RF amplifier, a detector diode, a DC amplifier, and a low-pass filter and integrator unit. Figure 1 shows a schematic of the instrument. Shared with the other radiometers were an analog-to-digital converter, a digital tape recorder and an on-line computer for real time analysis. The temperature of the receiver was kept constant by a thermal heating circuit, whose power is completely decoupled from the electronics power. The relevant parameters of the receiver are reported in Table 1.

We used a conical corrugated horn antenna, which provides excellent E- and H-plane beam symmetry and low sidelobes (less than -50 dB at angles greater than 70°). The horn is the same one used for the 4.75 GHz measurements in the first phase of the collaboration, and has been described in detail elsewhere (Bielli *et al.* 1983). The measured beam pattern at 3.7 GHz is found to be in good agreement with the theoretical predictions.

The front-end amplifier is a commercial unit for home satellite reception, which we modified for our needs. The absence of a microwave switch and of a mixer makes the first amplifier's noise the dominant element of the total system noise (84 K). The highpass filter reduces interferences and system noise originating from low frequency signals. A second RF amplifier was used to increase the signal power at the detector diode and to reduce the amount of DC gain needed.

To compute the center frequency and the equivalent bandwidth of the radiometer, we integrated the bandwidth of the amplifiers, weighting each frequency interval by its average gain, and then determined the center frequency and the width of an ideal amplifier having constant gain across its passband, and of equivalent total gain.

IV. MEASURING SITE

The experiment was carried out, as in previous years, at the Nello Pace Laboratory of the University of California's White Mountain Research Station. The Laboratory lies on a mountain plateau, 3800 meters above sea level, at a latitude of 38° N. The area is in the rain shadow of the Sierra Nevada mountain range in eastern California. Typical atmospheric water vapor content (the dominant source of variability in atmospheric antenna temperature) at the site is low (≤ 5 mm of precipitable water) during clear summer nights. Data with LHe in the dewar were taken during the nights of 8 and 9 August 1986 (UT). In the same period, our group operated other receivers at 90, 10, and 1.4 GHz. Results from those measurements have been reported by Smoot *et al.* (1987a).

V. DATA TAKING AND PROCESSING

a) *Atmospheric and galactic measurements*

An atmospheric measurement consisted of several (typically 10) scans. Each atmospheric scan consisted of five position/target combinations as reported in Table 2. Occasionally, warm eccosorb was used also at the 31° and 41° positions, to check that the radiometer gain stayed constant throughout the different positions. The 31° and 41° pointing angles were nominal; upon measurement, the angles from zenith were found to be $31^\circ 9'$, and $41^\circ 43'$, with a measurement uncertainty of $\pm 5'$, and a repeatability uncertainty of $\pm 20'$.

Measurements of the atmospheric emission were made at several different times each night, but not during the time of overhead transit of the galactic disk. During this period (approximately between 3 and 7 UT), differential profiles of the galaxy were obtained by tipping the receiver between the vertical and 31° positions.

b) *Zenith sky measurements*

Measurements of the zenith sky temperature were done twice per night during the nights of 8 and 9 Aug (UT). Each measuring period lasted approximately 50 minutes. The measuring routine called for the receiver to view alternately three different loads: the vertical sky, an ambient temperature eccosorb target (used as a warm load), and the cold load. The loads were alternated according to a fixed scheme: sky, cold load (with radiometer turned upside down), sky, warm load. Each sequence of 4 positions constitutes a scan. Rotation of the radiometer took less than 4 seconds, so that most of the time (32 sec) allocated for each position could be used to accumulate the signal.

c) *Integration and monitoring*

The radiometer output was integrated over a 2 second period by the built-in integrator, and then digitized and recorded on cassette tape. Each target was observed for 16 periods (32 seconds); after digital integration the resulting r.m.s. (generated by the system noise) is just above 0.002 K. The data were monitored in real time to make sure that the receiver was working properly. After returning to Berkeley, we averaged together the data from each position during each scan. The integration allowed enough dead time between positions so that spurious signals generated by unwanted loads (e.g. ground seen during movement of the receiver) could safely be weeded out. Data from all the scans were averaged by the position to which they refer; if just one position in a scan showed a large r.m.s., the data from the entire scan were discarded.

d) Radio frequency interference

Intrinsic in the design of the receiver is the problem of radio frequency interference (RFI). Geosynchronous satellite transmitters in the popular 3.7-4.2 GHz TV band can produce a large (80 K or more) signal when viewed directly. The directivity of our antenna is sufficient to reduce their signal to low levels ($\leq 0.01K$), provided the receiver is pointed to the zenith. Other sources of interference are local microwave links, and ground based and airborne radars. Such interference is more difficult to identify and screen against, since it can come from any direction, at any time, and at any power level. At the experimental site we scanned the horizon to the north and east with a spectrum analyzer and a receiver with a broad beam antenna, to make sure that no unwanted signal was received. Since RFI was still present, we used the radiometer itself as a directional receiver, in order to find an interference-free direction. We decided to do atmospheric scans along a plane at $76 \pm 2^\circ$ from the geographic north, where RFI was below the level of detectability ($\leq 0.005 K$). Commercial jets use radar altimeters in the 4.2-4.4 GHz band. We kept a record of each jet we could see or hear, and threw away all data taken during the times of airplane overpass. The data discarded were often indistinguishable from nearby, undisturbed data. The percentage of contaminated data varies with local time, being maximum ($\approx 5\%$ of data) around 22:00 (PDT), and becoming almost null shortly after 01:00 (PDT).

VI. COLD LOAD TARGET

The cold load used in this experiment has been described previously (Smoot *et al.* 1985b) and has not been modified; its radiometric temperature is, to the first order approximation, the temperature of the cryogenic liquid in it. A more precise estimate can be obtained if we consider the effect of the materials and geometry of the load on the propagation of the radio signal. Table 3 summarizes each element and its contribution. De Amici *et al.* (1985) discuss in detail most of the entries in Table 3, and we will discuss here only the "coherent reflection" effect.

Due to the relatively narrow bandwidth of the receiver, signals emitted from the radiometer and reflected from the target can interfere coherently with internal reflections in the radiometer. If both the target and internal reflectivity are small, then reflections can be written as:

$$T_{refl} = T_{in} \left(R_{target} + R_{internal} + 2 (R_{target} R_{internal} \cos^2 \Theta)^{1/2} \right) \quad (3)$$

where T_{refl} is the temperature of the reflected signal, T_{in} is the broadcast signal's temperature, R_{target} and $R_{internal}$ are the power reflection coefficients for external and internal reflections, and $\cos \Theta$ is a phase factor depending on the geometry of the reflection. The factor $\cos \Theta$ is averaged over the coherence length. The first term on the right is small, and the second term cancels out in our differential measurement; if $R_{internal}$ is larger than R_{target} , then the third term

on the right can become the dominant one. We were unable to measure the amplitude and phase of the reflection over the cold load. Tests with a simulated cold load suggest an upper limit of 0.055 K; we used this value as the potential error in the temperature of the cold load.

VII. ATMOSPHERE

In order to minimize the potential systematic errors, the atmospheric contribution should be measured with the same instrument used for, and as close as possible to the time of, CBR measurements. During past experiments, the receivers have been mounted on carts, and have been designed so that all these requirements could be met (De Amici *et al.* 1985, Witebsky *et al.* 1986, Mandolesi *et al.* 1986, Sironi *et al.* 1987). The 3.7 GHz radiometer, however, was not mounted on a cart, and the structure for atmospheric scans could not be easily moved. We made atmospheric measurements with this receiver as close in time as possible to any LHe scans; the 10 and 90 GHz receivers made additional atmospheric scans while the 3.7 GHz receiver was taking zenith sky data.

Each scan yielded an atmospheric temperature for the 31° and 41° zenith angle. Statistical uncertainty is twice as large for the 31° values, than for the 41° ones, and total uncertainty (which is dominated by systematics) scales in the same way. The two values were averaged together, with weight proportional to the statistical uncertainty. The average constitutes a scan's result. The scans were then averaged together to give a value for a measurement.

The results of all atmospheric measurements are reported in Table 4. Figure 2 shows the histogram of the results of all atmospheric scans. Typically, each point has an intrinsic uncertainty, due to both statistical and systematic errors; the latter, which apply equally to all data, will be discussed later. Because of the shape of the distribution of the data the data have not been weighted by their systematic error. The systematic error of the average is taken to be the largest between the systematic errors at 31° and 41°.

a) *Statistical errors*

The errors listed in Table 4 are r.m.s. variations of the individual points. Since the differential signal is as small as 0.15 K, corresponding to 15 digitized units, digitization problems in the ADC might play a significant part in the overall error budget. These errors, however, can be expected to occur randomly, and their importance decreases as more and more measurements are taken. During a measurement, the data are quite consistent with each other, and the statistical error is small; however, when different measurements are compared, the difference is comparable to the r.m.s. error of a single measurement.

Figure 2 shows the data from all scans. The average of all scans gives $T_{aim} = 0.871$ K, with an r.m.s. scatter in the data of 0.197 K, while the average of all measurements (as reported

in Table 4) gives $T_{atm} = 0.870$ K with an r.m.s. of 0.148 K. It should be noted that this uncertainty is larger than the spread in the data expected from computations based on atmospheric models; the atmospheric emission is expected to be stable with time at 3.7 GHz. The fit of the data to a gaussian distribution is poor; however, the averages of different subsets of the atmospheric scans do not deviate by more than 0.01 K from the average for the total set. If the same procedure is applied to the measurements, then the deviation becomes 0.014 K. This suggests that 0.870 K is a good estimate of the mean of the parent distribution. For the uncertainty on this value, we took the 10 measurements reported in Table 4, and computed a statistical uncertainty for their average. Apart from the distribution, there is no indication of problems in the data; a possible explanation is that RFI was being intermittently received. Our best and most sensitive RFI detector is the radiometer itself; RFI tests conducted before and after data-taking routines do not yield absolute certainty of what was going on in the time between tests.

Our best estimate of the temperature of the atmosphere, with statistical uncertainty only, is:

$$T_{atm} = 0.870 \pm 0.049 \text{ K}$$

b) *Systematic errors*

In an idealized model (flat atmosphere, pencil-like beam, negligible self-attenuation), the atmospheric signal is proportional to the secant of the pointing angle, and can therefore be easily determined. Under actual conditions, allowance has to be made for the finite size of the antenna beam, the curvature of the atmosphere and its temperature distribution, attenuation of the signal, and diffraction of ground emitted signal over the ground screens and into the antenna (Witebsky *et al.* (1986) give a complete discussion of these phenomena, and describes the measurement technique). At this frequency, these effects cause corrections of 2%, 0.2%, $10^{-5}\%$, $10^{-3}\%$, and 5% of the measured signal, respectively.

Other systematic errors in the atmospheric antenna temperature come from uncertainties in measurement of receiver gain, in pointing angle of the horn, and in galactic corrections. Table 5 summarizes the contribution of each element.

The atmospheric model uses two parameters: scale height and physical temperature of the atmosphere. In this analysis, we used a scale height of 6 km, and a temperature of 260 K. At 3.7 GHz, however, the atmosphere is optically thin, and large variations of the parameters do not affect the result of the measurements. For a 2 km variation in scale height or 20 K variation in kinetic temperature, the atmospheric antenna temperature changes by less than 0.001 K.

The beam pattern measured in Berkeley was used for fitting the atmosphere. We repeated our analysis assuming a gaussian beam of equal HPBW, and others slightly (3°) wider and narrower, and found that the atmospheric emission did not change by more than 0.020 K in

either case. The test cases provide conservative upper and lower limits to the possible differences of our measured beam from the real one.

To minimize the ground-emitted signal which enters the receiver through the antenna sidelobes, we used an antenna with very low sidelobes, and a set of screens to intercept and redirect to the sky the part of the beam which would otherwise see the ground. Theoretical computation of ground contribution is possible, if the antenna gain pattern is well known and the horizon profile has been accurately measured. We preferred to measure the ground contribution directly, in the same location and receiver positions as used during CBR and atmospheric measurements. The technique consists of successively adding layers of ground screens, which would be impractical to use during the real experiment, until the next layer has no effect on the receiver's output. The screens are then taken down, and the signal difference is a measure of the ground contribution. In order to reduce the effect of gain changes and drifts, the procedure is repeated many times, and the average of the data is taken. Direct measurements, however, are not free from problems: since the ground signal can diffract over the edge of the screens, their geometry must be carefully considered; in some cases, additional ground screens have been shown to increase up to 0.050 K the diffracted signal received by the radiometer. Rough estimates of the expected ground signal can be obtained by modelling the diffraction around the edge as a diffraction through a slit, whose width is $1/2$ the wavelength, and by estimating, from geometrical considerations, the gain-weighted fraction of the antenna beam that sees the slit. This approximation agrees quite well with direct measurements, and allows us to estimate the residual ground signal when size makes it impractical to add additional screens. The direct measurement of contribution from the sidelobes also puts an upper limit on the amount of RFI signal being received from time-independent sources, such as geostationary satellites. We measured a sidelobe contribution of 0.020 ± 0.004 K when looking to the zenith, 0.038 ± 0.007 at 31° , and 0.045 ± 0.008 at 41° . The data have been corrected for this effect, and the uncertainties (added in quadrature) taken as the uncertainty of the correction.

Changes in radiometer system noise between the vertical and 31° and 41° positions were measured by looking at the same target (a piece of warm eccosorb) in the three positions. The signal was found to be constant within 0.003 K. If we assume that the change comes from changes in system temperature, then the uncertainty in the atmospheric emission is less than 0.018 K. If the signal change is due to gain changes, then the resulting uncertainty is negligible (less than 0.001K).

The calibration constant G is measured from the difference in signal between two loads at widely different and well known temperatures (usually an ambient target and a cold one), after allowing for saturation effects in the amplification and detection chain. The timescale of the measurements is so short that drifts in gain, which we measured to be less than 0.3% over a 17-

minute time period, become negligible. Errors in measurement of the calibration constant come from uncertainties in the temperatures of the loads, and statistical fluctuation in the output of the receiver (Table 6). Their combined effect results in a fractional error of less than 0.4%. Since $T_{atm} \approx 0.9$ K, the resulting error is less than 0.004 K.

Errors also arise from saturation of the detector. We measured the response curve, as defined by the change in output for a known change in input, of the diode and DC amplifier together. A straight line fit through the low-input-power data yields the linear response curve for our receiver. We found that a best fit curve through the data is a second order polynomial, whose deviations from a straight line start being noticeable for input signals corresponding to about 70 K. The difference between the output voltages predicted, for the same input power, by the polynomial fit and the linear fit is a measure of the saturation effects in the detection and post-detection amplifying elements. For this experiment, we found a 22 (± 3)% decrease of signal when the radiometer is looking at eccosorb, and a 3.8 (± 0.5)% decrease when looking at sky or LHe. These corrections, in part, counteract each other, and their uncertainties tend to cancel out, leaving an error of ± 0.027 K.

Pointing angles were measured before (or after) each series of scans. The measurement uncertainty is less than 5 arcminutes, but the repeatability of the angles is questionable. Tests showed that the pointing angle could change by as much as 20 arcminutes from scan to scan. This uncertainty translates into a 2.4% error (± 0.023 K) in the value of T_{atm} measured at 31° , and 2.0% error (± 0.019 K) at 41° .

The galactic signal was computed from models and subtracted from the data; differences between model prediction and measurements (which will be discussed later) suggest an uncertainty of 0.030 K in this correction. After allowing for the differential character of our measurement, the error introduced in the atmosphere is ± 0.060 K.

Systematic errors have then been added in quadrature to the statistical uncertainty. The average antenna temperature of the vertical atmosphere and its uncertainty then become:

$$T_{atm} = 0.870 \pm 0.108 \text{ K}$$

c) Comparison with models

Different models exist (Costales *et al.* 1986, Liebe 1985) that allow one to compute the atmospheric antenna temperature as a function of frequency, altitude, water vapor content and kinetic temperature of the atmosphere. Using the measurements of atmospheric antenna temperature at 10 and 90 GHz that were done simultaneously with the 3.7 GHz zenith sky measurements, we can estimate the atmospheric water vapor content. The models predict atmospheric antenna temperatures between 0.83 and 0.87 K. Although not totally incompatible, the average of our measurements and the model predictions are, at best, in marginal agreement. The agreement does not improve if only data from the nights of 8 and 9 August are used; the

average atmospheric temperature then becomes 0.884 K, with an r.m.s. of 0.172 K, while the average of the first three nights of data is 0.856 K, with an r.m.s. of 0.137 K. It should also be noted that the model predicts signal variation that are much smaller than we experienced. The atmospheric antenna temperature depends on the amount of oxygen and water present in the atmosphere; since the oxygen is well mixed, short term changes in the atmospheric emission depend on changes in column density of water. At our frequency and from our site, the water is expected to contribute about 0.1 K to the total signal, and the short-time-scale variation, for a 20% change in column density, should be less than 0.03 K. As said before, intermittent RFI could be the cause of these discrepancies.

VIII. GALAXY

The galactic emission at 3.7 GHz is small; however, even away from the galactic plane it is not negligible (≥ 0.04 K). During the summer months the galactic plane, which represents the direction of maximum emission (≈ 0.4 K), passes overhead during the night. This implies that the signal from the zenith sky contains a galactic contribution, which depends on declination and right ascension of the direction of observation, and antenna beamwidth. This contribution can be estimated from galactic maps at 408 MHz (Haslam *et al.* 1982) and maps of HII sources, or measured directly. Figure 3 shows the computed galactic profile at 3.7 GHz, for a radiometer with beamwidth of 15° (HPBW) at a latitude of 38° N. Since the observing site is unreachable during the winter months, the problem caused by galactic emission cannot be avoided by design or planning.

We made direct measurement of the galactic emission by mean of differential scans, performed by moving the receiver between the zenith and the 31° positions. Calibrations with ambient temperature eccosorb were done at regular intervals. The difference in signal, after allowing for differential ground and atmospheric contribution, is due to the difference in galactic emission, and is a function of time:

$$\Delta T = G (V(0^\circ) - V(31^\circ)) = T_{gal}(0^\circ) - T_{gal}(31^\circ) = T_{gal}(\delta, RA) - T_{gal}(\delta, RA+2.07) \quad (4)$$

where RA is the right ascension, in hours, at the moment of observation, δ ($=38^\circ$) is the latitude of the observing site (declination of the zenith), and 2.07 is the delay, in hours, due to the 31° pointing angle.

This technique only allows us to measure differences; its results can be affected by a constant offset, which in our experiment is the level of minimum galactic emission. It is still useful, however, since the results can be fit to a theoretically computed galactic profile and used to verify its accuracy, including an estimate of the offset.

Due to external constraints (horizon profile and RFI sources), our radiometer did not scan in the true east-west direction, but rather at an angle of 14° from it (cf. Table 1). This implies that (4) becomes:

$$\Delta T = T_{gal}(0^\circ) - T_{gal}(31^\circ) = T_{gal}(\delta', RA) - T_{gal}(\delta'', RA+2.01) \quad (5)$$

where δ' ($=38^\circ$) and δ'' ($=46^\circ$) refer to the declination of observation when the receiver is pointed to the zenith and away from it, respectively, and the delay, due to the geometry of the pointing, is now 2.01 hours.

The use of two different galactic declinations introduces additional sources of error and uncertainty. We compared the results of the experimental scans with those predicted by our galactic model, and used the fit to estimate the uncertainty in the model.

Figure 4 shows the results of our scans, superimposed over a simulated scan, derived from our galactic model. Each experimental point is the combination of the data from different nights, averaged in 5-minute wide bins. The agreement between model and measurement is good, although the intensity of the signal is somewhat smaller than expected (about 0.025 K smaller at the peak), and the time of transit is off by 7 minutes. The latter effect is likely due to a slight pointing error. Such a transit error, corresponding to a 0.5° error in pointing, is within the 2° precision of our azimuth pointing. The difference in amplitude could be easily explained by an underestimation of the thermal (HII) background, or by an error in the spectral index α used in our model for the synchrotron radiation. We assumed $\alpha = 2.75$; if it is $\alpha = 2.80$, then the difference between model and data would almost disappear.

IX. ZENITH SKY TEMPERATURE

The temperature difference between vertical sky and cold load was determined from the data, after accounting for the receiver's calibration constant, and subtracting the galactic signal, as computed from our model. Table 7 and Figure 5 show a summary of the results up to this stage.

As usual, errors can be divided into statistical and systematic. Table 8 summarizes the error budget for the CBR measurements. The histogram (Figure 5) of the results from all scans provides a good fit to a gaussian distribution; we computed the statistical error by averaging all the scans together. The resulting uncertainty is 0.008 K.

Some of the systematics (gain errors, atmospheric temperature errors, saturation correction) are, in principle, the same as those already treated when the atmospheric signal was being discussed, and will not be repeated here. Other effects are: position dependent changes in system temperature, cold load temperature uncertainty, and galactic corrections.

Changes in receiver system temperature that correlate with changes in receiver position, in this case with inversion of the receiver, are usually caused by changes in mechanical stresses on

the components (waveguides or coax), which in turn change the electrical properties (reflectivity and attenuation) of the microwave circuit. The radiometer was designed and built with this problem in mind; stiffening cross-elements have been added to its mechanical structure to make it stronger and less prone to bend under stress. We measured the dependance of the system output voltage upon position. A piece of eccosorb at ambient temperature was firmly attached to the horn, and we measured the output signal change when the radiometer was rotated upside-down. Care was taken to avoid any change in target's properties, which could modify the result of the test; special care was taken to be sure that neither the target temperature during rotation (such as if it were going from sunshine to shade), nor its distance from the horn nor its shape did change. The low level of system noise and the digital integration of the radiometer output for long intervals allowed us to obtain very small errors in the measurements. The tests indicated that the receiver output increased by -0.035 ± 0.020 K when it was rotated upside-down, with the uncertainty coming mostly from spread of experimental results. While this is probably due primarily to changes in the target or calibration constant, we adopt it for our measurement of ΔT_{sys} . If we use this value as a measurement of gain variations, as stated in eq. (2), then the uncertainty introduced in our result would become just 0.011 K.

Galactic corrections for the vertical sky brightness during CBR measurements were computed from the model, and subtracted from each single scan. The galactic signal ranged from 0.059 to 0.076 K, and we took as uncertainty 0.030 K, to account for both model and data uncertainties. Cold load temperature uncertainties have been discussed previously, and are listed in Table 3.

X. TEMPERATURE OF THE CBR

Combining equations 1 and 2 gives

$$T_{A,CBR} = G (S_{zenith} - S_{load}) + T_{A,load} - \Delta T_{sys} - T_{A,galaxy} - T_{A,ground} - T_{A,atm} \quad (6)$$

We now have all the elements to compute the temperature of the CBR. From eq. (6) and Table 9, we can write: $T_{A,CBR} = 2.49 \pm 0.13$ K or, converting to thermodynamic temperature:

$$T_{CBR} = 2.58 \pm 0.13 \text{ K}$$

where the error comes from the data in Table 9.

XI. DISCUSSION AND COMPARISON WITH PREVIOUS RESULTS

From the original measurement by Penzias and Wilson (1965) at 4.08 GHz, until the time our US-Italy collaboration was started, only one experiment had measured the temperature of the CBR between 2 and 9 GHz (Otoishi and Stelzried 1975, but data were taken in 1967). A full discussion of the results from the other receivers and the cosmological implications of our experiment is beyond the scope of this paper; Smoot *et al.* (1985b), De Amici *et al.* (1985), and

Smoot *et al.* (1987b) give an account of how the improved experimental results have narrowed the limits for spectral distortions. The results obtained at nearby frequencies by other experimenters are summarized in Table 10.

Our measurement's frequency falls halfway between those of Sironi *et al.* (1987), and Mandolesi *et al.* (1986). All these three experiments have been carried out from the White Mountain site, and their results tend to corroborate each other. It should be noted that the atmospheric temperature, as measured at 3.7 and 10 GHz in 1986, does not fit the atmospheric model fitted to the 2.5 and 4.75 GHz measurements (Sironi *et al.* 1987, Mandolesi *et al.* 1986), suggesting the possibility of a systematic offset in either set of data, or a substantial undetected difference in atmospheric conditions.

In this first year of operation the 3.7 GHz receiver performed well, yielding data of good quality. As the preceding discussion has shown, the precision of our measurement has been limited by the uncertainties in the atmospheric contribution, in the cold load radiometric temperature and in the galactic signal, in decreasing order of importance. We believe that the accuracy of our measurement of the last two effects can be greatly improved with some modification to the apparatus. A precise measurement of the atmospheric signal at our frequency, however, cannot be obtained unless we can find a direction of suitably low horizon profile free from RFI. This possibility is reduced every year, as more and more radars and microwave links are put in service. We might have to use a different receiver, working in a protected radioastronomical frequency band, to measure the atmospheric signal, and then extrapolate to our frequency.

If the major sources of uncertainties could be reduced by a factor of two, a goal that is attainable, then the overall experimental error would become ≈ 0.07 K; this would make our measurement one of the most precise ground-based determinations of the temperature of the CBR.

XII. ACKNOWLEDGMENTS

This research was partially funded by the Department of Energy Contract DE-AC03-76SF00098 and by the National Science Foundation Grant No. AST 8406187. We wish to thank John Gibson, Marc Bensadoun, Larry Levin, Faye Mitschang, and Carol Stanton for their help and support during the planning and realization phases of the experiment, and the crews and staff of the White Mountain Research Station, for making our stay at the high altitude site much more bearable than it could have otherwise been, and for their help fixing last minute problems. We also thank Dr. N. Mandolesi of CNR/Bologna for lending us the horn antenna used in this experiment. M.B. wishes to thank ISTR (Milano) for fellowship support.

 Table 1 - Relevant parameters of the 3.7 GHz receiver

center frequency	3.7 GHz	measured
wavelength	8.1 cm	computed
bandwidth	± 230 MHz	measured
system noise	84 ± 1 K (a)	measured
sensitivity	5.5 mK/sec ^{1/2}	w/cold and warm loads theoretical
	13 mK/sec ^{1/2}	measured
beamwidth (HPBW)	15°	w/eccosorb target measured
pointing: angles from vertical	$0^\circ 32' \pm 5'$	measured
	$31^\circ 09' \pm 5'$	measured
	$41^\circ 43' \pm 5'$	measured
pointing: angle from geographic North	$76 \pm 2^\circ$	measured
RF gain	62 dB	measured
DC gain	300x	measured

(a) peak-to-peak variation of measured values

 Table 2 - Position-target sequence for atmospheric measurements

radiometer position	target
vertical	zenith sky
31° from vertical	sky 31° from zenith
41° from vertical	sky 41° from zenith
vertical	zenith sky
vertical	warm eccosorb

 Table 3 - Radiometric temperature of the cold load

quantity	contribution to temperature [K]	error [K]
cryogenically cooled target emission	3.695	0.004
windows and gas insertion loss	0.013	0.007
walls insertion loss	0.007	0.005
incoherent reflection	0.020	0.010
coherent reflection	0.000	0.055
total	3.735	0.057

 Table 4 - Results of atmospheric measurements during August 1987.
 Final value is the average of the averages of each measuring scan.

day	time [UT] from:	to:	samples	average signal and r.m.s.[K]	
5	10:01	10:22	6	0.701	0.062
5	10:46	11:05	5	0.781	0.098
6	3:31	3:58	7	1.056	0.060
6	9:37	10:06	9	0.820	0.038
7	2:45	3:13	11	0.926	0.083
8	2:44	3:10	7	1.115	0.077
8	8:56	9:09	3	0.806	0.029
8	10:37	10:55	5	0.992	0.035
9	8:25	8:54	8	0.672	0.078
9	10:10	10:36	8	0.835	0.060

average of the 10 measurements (and r.m.s. spread): 0.870 ± 0.148

 Table 5 - Error budget for atmospheric antenna temperature evaluation

quantity	amount	kind of error	effect on $T_{\text{atmosphere}}$
spread of data	0.870 ± 0.049 K	statistical	0.049 K (a)
atmospheric scale height	6 ± 2 km	systematic	0.001 K
atmospheric physical temperature	260 ± 20 K	systematic	0.001 K
diffracted earth radiation	± 0.008 K	systematic	0.048 K
pointing error	$\pm 20'$	systematic	0.023 K
gain error	$\pm 0.4\%$	systematic	0.004 K
saturation corrections	$\pm 3\%$	systematic	0.027 K
beam pattern	$\pm 3^\circ$ HPBW	systematic	0.020 K
galactic correction	± 0.030 K	systematic	0.070 K
radiometer offset change	± 0.003 K	systematic	0.018 K
total systematics			0.096 K
total errors			0.108 K

(a) taking all data from 5 to 9 august (see text)

 Table 6 - Sources of uncertainty in the measurement of the receiver gain

quantity	amount	error (68% c.l.)	% error on gain
temperature of cold load	3.74 K	$\pm 0.05\text{K}$	0.018
temperature of warm load	280 K	$\pm 1\text{K}$	0.362
signal of cold load	7000 d.u. (a)	± 3 d.u. (b)	0.014
signal of warm load	29000 d.u. (a)	± 3 d.u. (b)	0.014

(a) d.u. = digitized unit

(b) upper limit

 Table 7 - Difference between vertical sky and cold load calibrator antenna temperatures, after correcting for galactic signal, but before subtracting sidelobes or offset changes. Final value is the average of all data points, with rms uncertainty.

day and time (UT)	number of data points (a)	difference [K]	
		average	r.m.s.
8 Aug 03:40-04:34	18 (7)	-0.376	0.079
8 Aug 09:29-10:30	20 (8)	-0.376	0.049
9 Aug 09:09-10:01	21 (3)	-0.381	0.062
9 Aug 11:06-12:02	12 (14) (b)	-0.389	0.053
average of all scans		-0.380 ± 0.061	

(a) in parentheses the number of scans rejected

(b) during the last part of the measuring period, LHe level in the cold load fell below the top of the eccosorb; those data, for a total of 14 scans, have been discarded.

 Table 8 - Error budget for zenith sky measurements

quantity	kind of error	error amount [K]
spread of data	statistical	0.008 (a)
gain error	systematic	0.011
saturation corrections	systematic	0.007
RFI	systematic	0.010
total		0.018

(a) this uncertainty is the r.m.s. given in Table 7, divided by $(N-1)^{1/2}$; where N is the number of scans.

 Table 9 - Summary of data for measurements of antenna temperature of CBR.

quantity	amount [K]	error [K] (68% c.l.)
atmospheric temperature	0.870	± 0.108
sidelobes	0.030	± 0.007
position dependent output change	-0.035	± 0.020
cold load temperature	3.735	± 0.057
galactic emission	0.066	± 0.030
difference between cold load and sky	-0.314	± 0.018
total (according to eq. 6)	2.490	± 0.129 (a)

(a) errors have been added in quadrature

 Table 10 - Other CBR measurements between 2 and 8 GHz

reference	frequency [GHz]	$T_{V,atm}$ [K]	T_{CBR} [K]
Otoshi <i>et al.</i> (1975)	2.3	2.27 ± 0.20	2.66 ± 0.25
Sironi <i>et al.</i> (1987)	2.5	0.95 ± 0.05	2.77 ± 0.13
this work	3.66	0.87 ± 0.11	2.58 ± 0.13
Penzias <i>et al.</i> (1965)	4.08	2.3 (sic)	$3.3 \pm 1.$
Mandolesi <i>et al.</i> (1986)	4.75	0.997 ± 0.060	2.70 ± 0.07

References

- Bielli, P., Pagana, E., and Sironi, G., 1983, *Proceedings ICAP*, **1**, 509.
 Costales, J., *et al.*, 1986, *Radio Science*, **21**, 47.
 Danese, L., and De Zotti, G., 1982, *Astron. Astroph.*, **107**, 39.
 De Amici, G., Smoot, G., Friedman, S.D., and Witebsky, C., 1985, *Ap. J.*, **298**, 710.
 Haslam, C.G.T., Salter, C.J., Stoffel, H., and Wilson, W.E., 1982, *Astr. Astroph. Suppl. Ser.*, **47**, 1.
 Levin S.M., 1987a, Ph.D. thesis, University of California, Berkeley
 Levin S.M., *et al.*, 1987b, in preparation
 Liebe, H.J., 1985, *Radio Science*, **20**, 1069.
 Mandolesi, N., Calzolari, P., Cortiglioni, S., and Morigi, G., 1984, *Phys. Rev. D*, **29**, 2680.
 Mandolesi *et al.*, 1986, *Ap. J.*, **310**, 561.
 Meyer, D.M., and Jura, M., 1984, *Ap. J. (Lett.)*, **276**, L1.
 Ootshi, T.Y., and Stelzried, C.T., 1975, *IEEE Trans. Instr. Meas.*, **24**, 174.
 Partridge, R.B., *et al.*, 1985, *Conference Proceedings, Societa' Italiana di Fisica*, **1**, 7.
 Penzias, A.A., and Wilson, R.W., 1965, *Ap. J.*, **142**, 419.
 Peterson, J.B., Richards, P.L., and Timusk, T., 1985, *Phys. Rev. Lett.*, **55**, 332.
 Sironi, G., and Bonelli, G., 1987, *Ap. J.*, in press.
 Smoot, G., *et al.*, 1985a, *Conference Proceedings, Societa' Italiana di Fisica*, **1**, 27.
 Smoot, G., *et al.*, 1985b, *Ap. J. Lett.*, **291**, L23.
 Smoot, G., 1986, in: J.P. Swings (edt.) *Highlights of Astronomy*, (Reidel, Hingham), 297.
 Smoot, G., *et al.*, 1987a, *Ap. J. Lett.*, in press
 Smoot, G., *et al.*, 1987b, in preparation
 Witebsky, C., Smoot, G., De Amici, G., and Friedman, S.D., 1986, *Ap. J.*, **310**, 145.
 Woody, D.P. and Richards, P.L., 1981, *Ap. J.*, **248**, 18.

Figure captions

1 - Schematic diagram of the 3.7 GHz radiometer.

2 - Distribution of the data on atmospheric antenna temperature. Histograms are shown for the whole set of data taken between 5 and 9 Aug. 1986 (UT), and for the subset taken during the nights of 8 and 9 Aug 1987 (UT).

3 - Galactic profile at 3.7 GHz, for the declination 38° N. The profile has been obtained from extrapolation of the map at 408 MHz (Haslam *et al.* 1982) and of a compilation of sources at 2.5 GHz, and has been fitted to a 15° HPBW antenna. The declination of 38° North corresponds to the zenith of our experimental site

4 - Results of differential galactic drift scans at 38° and 46° declination, and prediction of a similar scan obtained from the galactic model. Data from the model have been corrected for atmospheric emission (assuming $T_{\text{atmosphere}} = 0.870$ K); a 0.1 K error in atmospheric temperature shifts the level of the curve by 0.015. Experimental data have been corrected for ground contribution and binned in 5-minute intervals (≈ 28 data points/bin). Time of observation has been normalized to an arbitrarily chosen date (6 Aug 1986). Error bars shown are typical.

5 - Histogram of all CBR measurements after galactic corrections, but before atmospheric emission, sidelobe contribution and cold load temperature have been subtracted. Data are shown as difference between cold load and zenith sky.

Jon Aymon, Marco Bersanelli, Giovanni De Amici, Al Kogut, Steven M. Levin, George F. Smoot, Chris Witebsky
50/232 Lawrence Berkeley Laboratory
1 Cyclotron Road
Berkeley, CA 94720

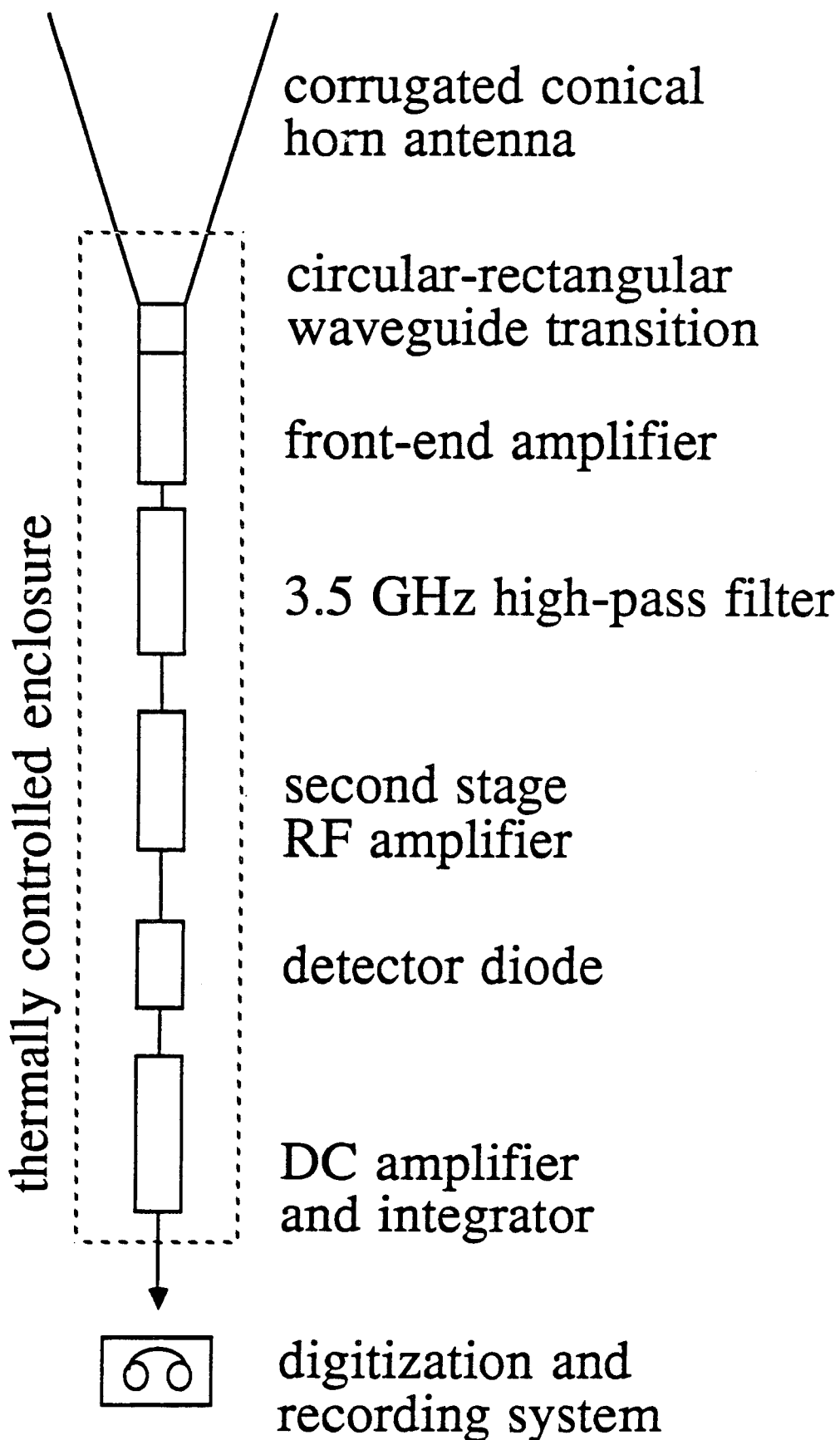


Fig. 1

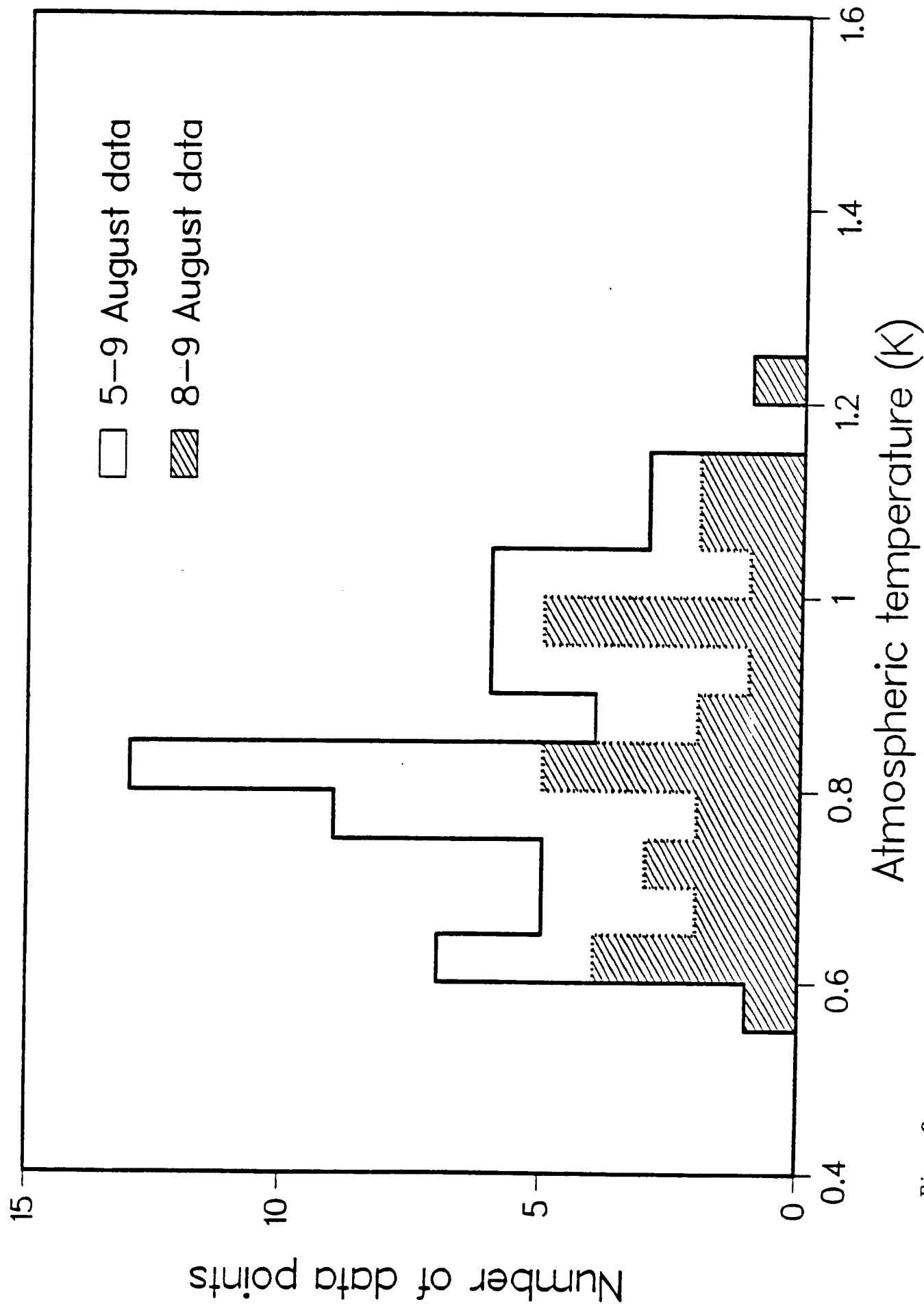


FIG. 2

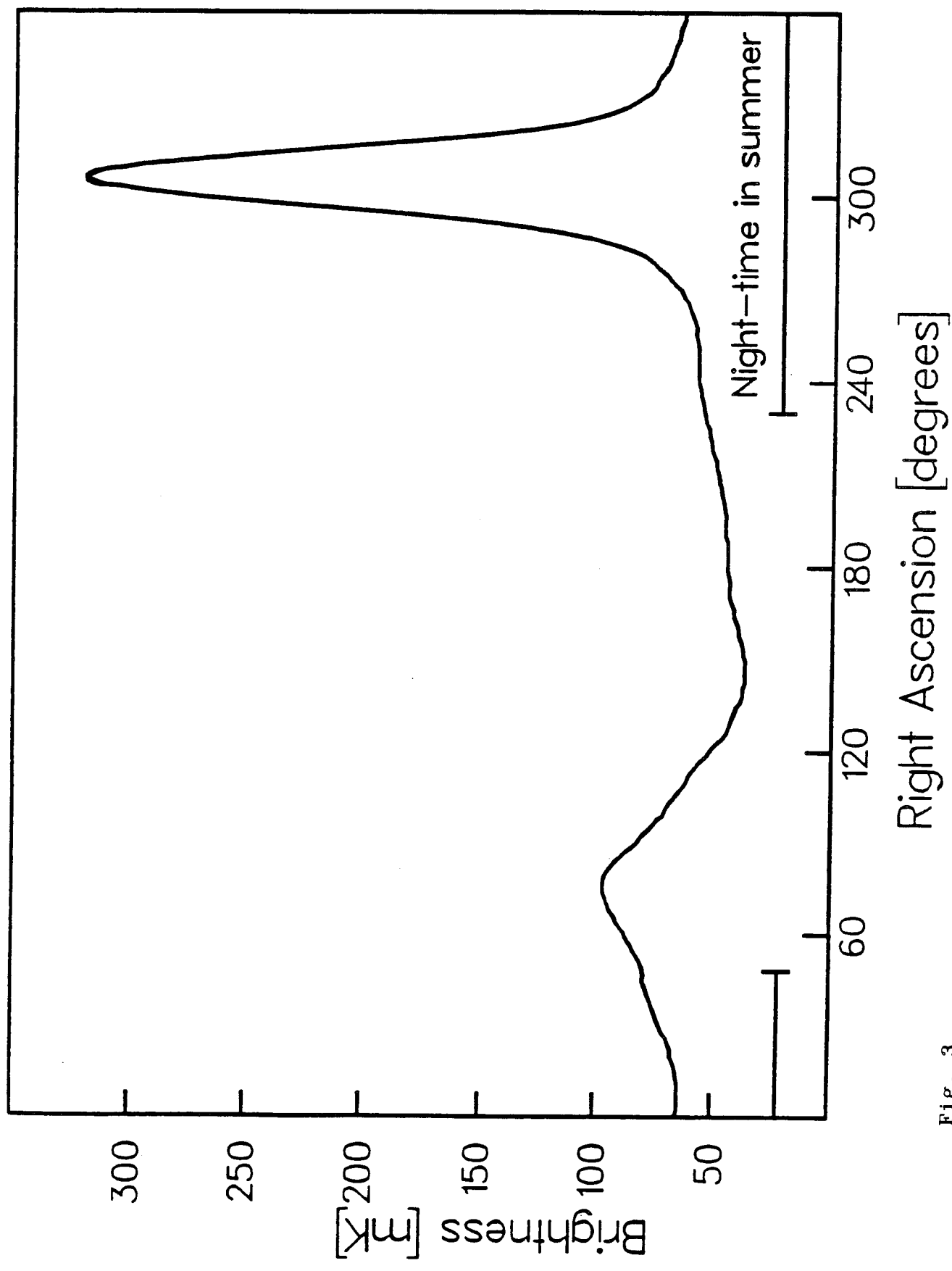


Fig. 3

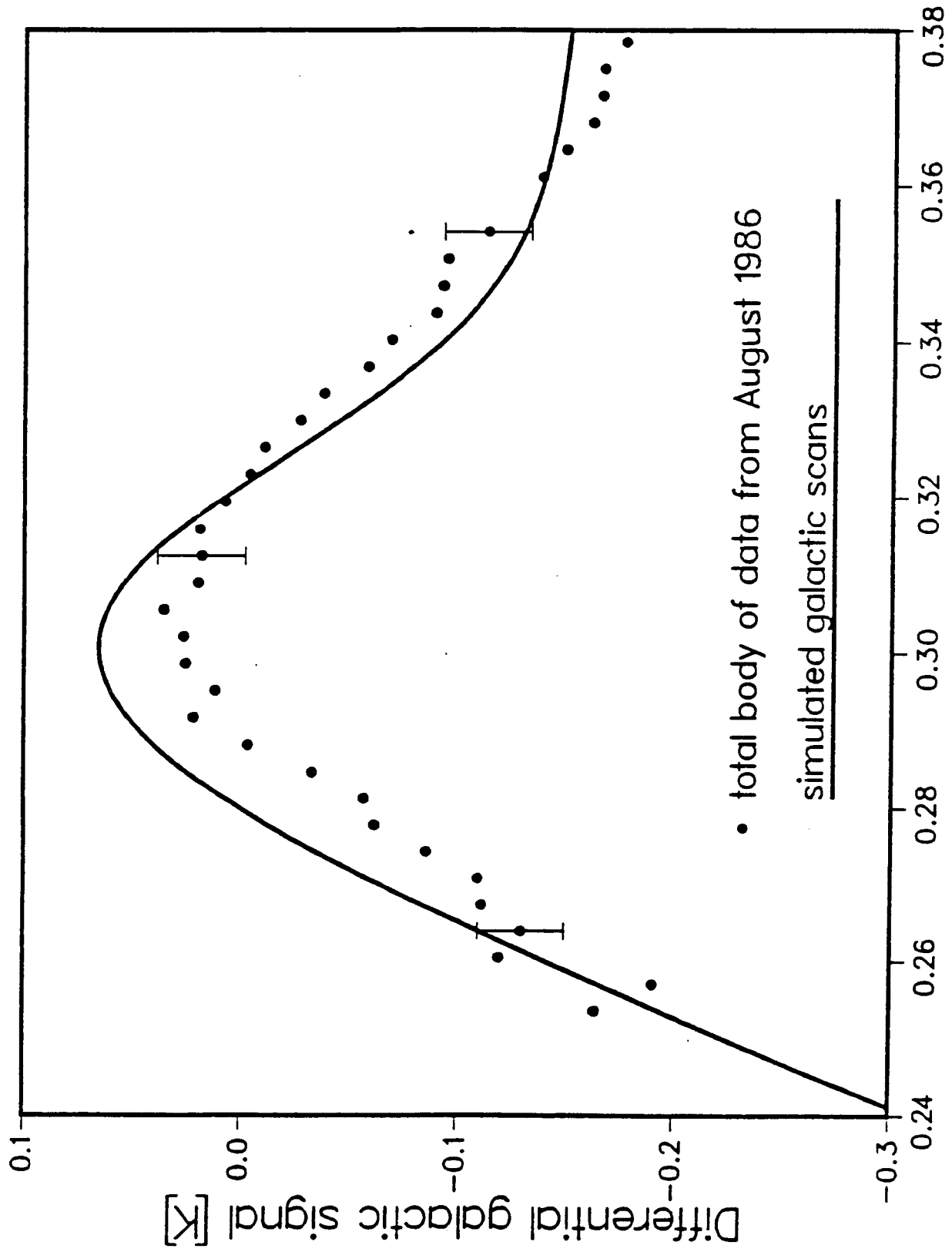


Fig. 4

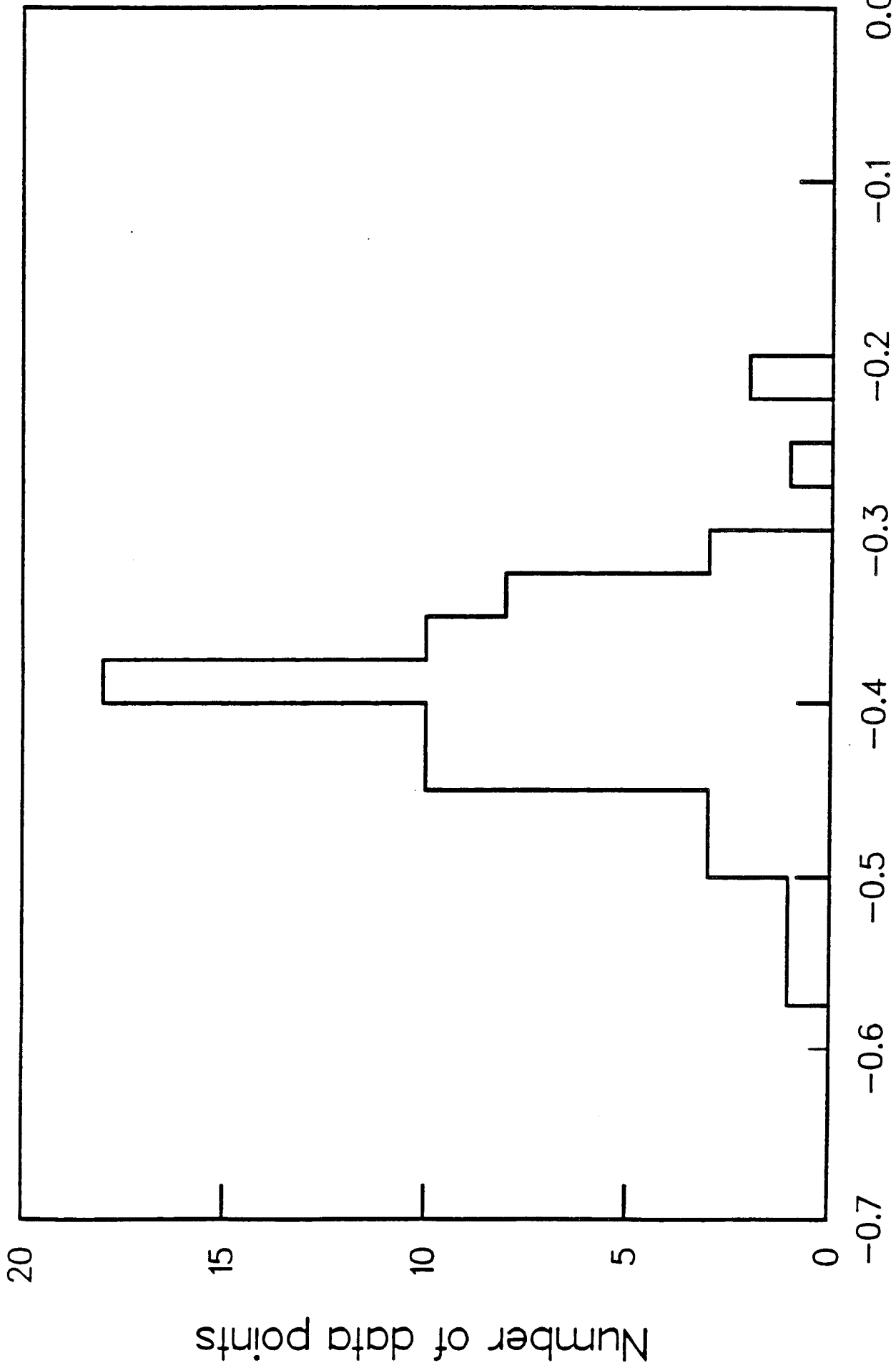


Fig. 5